Check for updates

Geophysical Research Letters

RESEARCH LETTER
10.1029/2025GL120829

# Unraveling the Source Locations of Short-Period Secondary Microseisms

**Samuel Jorde[1,2], Martin Schimmel[1], Eleonore Stutzmann[3], Zongbo Xu[3,4], Pilar Sánchez-Pastor[1], Helena Seivane[1,5], and Jordi Díaz[1]**

[1]Geosciences Barcelona (GEO3BCN), CSIC, Barcelona, Spain, [2]Departament de Dinàmica de la Terra i de l'Oceà, Facultat de Ciències de la Terra, Universitat de Barcelona, Barcelona, Spain, [3]Université Paris Cité, Institut de physique du globe de Paris, CNRS, Paris, France, [4]Norwegian Geotechnical Institute, Oslo, Norway, [5]Observatorio Vulcanológico y Sismológico de Costa Rica (OVSICORI-UNA), Universidad Nacional, Heredia, Costa Rica

**Abstract** Primary and secondary microseisms are generated by ocean wave interactions, with the latter occasionally split into short- and long-period bands in some regions. The short-period secondary microseism (SPSM) sources have traditionally been associated with nearby coastal segments, suggesting a more uniform distribution across shorelines. Here, we challenge this assumption by combining polarization analysis, source mechanism modeling and attenuation assessment in the Mediterranean Sea. This region offers an optimal setting, as we reveal that the primary and long-period secondary microseisms originate in the North Atlantic Ocean, whereas the SPSM arise within the Mediterranean Sea, allowing these sources to be clearly isolated. We find that SPSM sources are well-constrained, spatially localized and highly dynamic. Our results reveal that bathymetry strongly controls the spatial distribution of these sources.

**Plain Language Summary** Ocean waves can interact and generate seismic vibrations called microseisms. These microseisms include different types, and one of them, has long been thought to come mainly from nearby coastal areas, more or less evenly along shorelines. In this study, we test that idea using advanced methods to locate and analyze the sources of this signal in the Mediterranean Sea. This region provides an ideal case study because the other types of microseisms come from the Atlantic Ocean and can be clearly distinguished from our target signal, located in the Mediterranean Sea. We find that these sources occur in specific, dynamic areas strongly influenced by the shape of the seafloor. Our findings reveal that underwater topography plays a key role in where these signals form and a similar behavior is likely to occur in other parts of the world.

**Key Points:**

- Primary and long-period secondary microseisms recorded across the Mediterranean region originate from the North Atlantic Ocean
- Combining Rayleigh-wave polarization and source modeling allows precise localization of short-period secondary microseism (SPSM) sources
- SPSM sources are spatially localized and strongly controlled by bathymetry

**Supporting Information:**

Supporting Information may be found in the online version of this article.

**Correspondence to:**

S. Jorde,
sjorde@geo3bcn.csic.es

**Citation:**

Jorde, S., Schimmel, M., Stutzmann, E., Xu, Z., Sánchez-Pastor, P., Seivane, H., & Díaz, J. (2026). Unraveling the source locations of short-period secondary microseisms. *Geophysical Research Letters*, *53*, e2025GL120829. https://doi.org/10.1029/2025GL120829

Received 4 DEC 2025
Accepted 4 JUN 2026

**Author Contributions:**

**Conceptualization:** Samuel Jorde, Martin Schimmel
**Data curation:** Samuel Jorde, Zongbo Xu
**Formal analysis:** Samuel Jorde, Martin Schimmel, Eleonore Stutzmann, Zongbo Xu
**Funding acquisition:** Martin Schimmel, Jordi Díaz
**Investigation:** Samuel Jorde, Martin Schimmel, Eleonore Stutzmann, Pilar Sánchez-Pastor
**Methodology:** Samuel Jorde, Martin Schimmel, Eleonore Stutzmann, Zongbo Xu, Jordi Díaz
**Project administration:** Martin Schimmel, Jordi Díaz
**Resources:** Jordi Díaz

© 2026 The Author(s).
This is an open access article under the terms of the Creative Commons Attribution-NonCommercial License, which permits use, distribution and reproduction in any medium, provided the original work is properly cited and is not used for commercial purposes.

## 1. Introduction

Seismic noise is recorded globally and its general spectral structure exhibits consistent features across different locations (e.g., Stutzmann et al., 2009). This spectrum primarily consists of hum and microseisms, both of which occur at frequencies below 1 Hz. Microseismic noise is divided into primary (PM) and secondary (SM) microseisms, both generated by ocean wave interactions and consisting of body and surface waves, with Rayleigh waves carrying most of the energy (Haubrich & McCamy, 1969). PM, occurring mostly between 0.05 and 0.1 Hz, originates from ocean waves interacting with the sloping seafloor in shallow waters, producing seismic waves at the same frequency as the incident ocean gravity waves (Ardhuin et al., 2015; Hasselmann, 1963).

The SM is the most energetic noise signal below 1 Hz ranging from 0.1 to 0.5 Hz. It is generated in deep water when swells with similar frequencies but opposite directions interact, producing colliding waves at twice the frequency of the individual ocean waves (Hasselmann, 1963; Longuet-Higgins, 1950). The resulting pressure fluctuations near the ocean surface propagate within the water column, couple into the seabed, and thus propagate through the solid Earth. Water column resonances, controlled by bathymetry and seafloor structure, modulate the source amplitude, constituting the source site effect (Meschede et al., 2017; Obrebski et al., 2012; Xu et al., 2025).

This mechanism is widely accepted in the scientific community and supported by numerous studies on numerical models of SM source mechanisms (Ardhuin et al., 2011; Gualtieri et al., 2013; Stutzmann et al., 2012), coastal reflections (Gal et al., 2017), site effects (Gualtieri et al., 2014; Xu et al., 2025) and SM source location and characterization (e.g., Davy et al., 2015; Ermert et al., 2016; Ermert et al., 2017; Kedar et al., 2008; Möllhoff & Bean, 2016; Sergeant et al., 2013), among others.

**Software:** Samuel Jorde, Martin Schimmel, Eleonore Stutzmann, Zongbo Xu
**Supervision:** Martin Schimmel, Eleonore Stutzmann, Pilar Sánchez-Pastor, Jordi Díaz
**Validation:** Samuel Jorde, Martin Schimmel, Eleonore Stutzmann, Pilar Sánchez-Pastor, Helena Seivane
**Visualization:** Samuel Jorde, Pilar Sánchez-Pastor, Helena Seivane
**Writing – original draft:** Samuel Jorde
**Writing – review & editing:** Samuel Jorde, Martin Schimmel, Eleonore Stutzmann, Pilar Sánchez-Pastor, Helena Seivane, Jordi Díaz

Some studies have reported the emergence of a distinct signal at higher SM frequencies in certain regions including California (Koper & Burlacu, 2015), Hawaii (Bromirski et al., 2005) and Algeria (Schimmel et al., 2011), among others. In these cases, the SM spectrum exhibits a split, resulting in two distinct peaks: (a) the long-period secondary microseism (LPSM) from 0.1 to 0.2 Hz, and (b) the short-period secondary microseism (SPSM) from 0.2 to 0.5 Hz. The SPSM signal has been investigated from different perspectives, such as revealing strong correlations with local winds and wave heights (Borzì et al., 2025; Bromirski et al., 2005) and linking its generation to specific coastal segments (Diaz et al., 2025; Koper & Burlacu, 2015), intense storm activity (Borzì et al., 2024), or a nearly constant offshore distance (Xiao et al., 2022, 2025). Despite these advances, the detailed spatial distribution of these SPSM sources and the parameters that control this distribution remain incompletely understood.

In this study, we demonstrate that SPSM sources are well-constrained and spatially localized through distinct and independent methodologies. We also reveal the importance of bathymetry and convex shorelines in SPSM generation. Together, these results provide a comprehensive framework for understanding the regional controls and distribution of SPSM sources. We focus on the Mediterranean Sea as a case study, which offers three main advantages: (a) it is large enough to display significant spatial variability while maintaining dense azimuthal station coverage; (b) we find that the SPSM energy is confined and isolated within the Mediterranean Sea, as PM and LPSM originate in the North Atlantic Ocean, providing an exceptional opportunity to study SPSM sources; and (c) two broadband station profiles deployed in NE Iberia, one orthogonal and one parallel to the shoreline, are located near the coast with short interstation spacing, offering an optimal setup to study SPSM inland attenuation.

## 2. Data and Methods

### 2.1. Data

The data used in this study are obtained from various broadband stations around the western Mediterranean, operated by the Institut Cartogràfic i Geològic de Catalunya (CBRU, EMUR, CMAS), the Istituto Nazionale di Geofisica e Vulcanologia (CGL, RORO, LATE and CORL) and the Réseau Sismologique et Géodésique Français (SMPL and ARBF). We also use continuous data from two broadband profiles deployed in NE Iberia in April 2024 as part of the EPYSIM project (Diaz & Schimmel, 2024): one oriented NE–SW (parallel to the coast) composed of 10 stations, and another NW–SE (orthogonal to the coast) with 9 stations.

### 2.2. Rayleigh-Wave Polarization of Microseisms

In order to locate SPSM sources, we follow a Rayleigh-wave polarization approach. For this purpose, we take advantage of the fact that microseisms are primarily composed of Rayleigh waves. This method also allows us to determine whether the recorded SPSM energy arrives from preferred directions rather than being uniformly distributed along the shoreline. To this end, we preprocess the seismic data by downsampling to 10 Hz, deconvolving the instrument response, removing the mean and trend, applying a broad band-pass filter between 0.03 and 5 Hz and segmenting all three components into 12-min traces. Finally, the Rayleigh-wave polarization analysis is performed in the three frequency bands corresponding to each one of the microseismic peaks identified in the spectra recorded at regional stations (Figure S1 in Supporting Information S1): (a) 0.05–0.1 Hz for PM, (b) 0.1–0.25 Hz for LPSM, and (c) 0.25–0.5 Hz for SPSM. Although the frequency content of each microseismic peak varies over time, for instance, between winter and summer (Figure 1a) or in response to individual storms that may generate higher or lower frequency content at a given time, these frequency ranges capture most of the energy of each microseism throughout the year. Moreover, since this is a full-year analysis, occasional outliers caused by individual storms do not affect the final results.

The method, described by Schimmel et al. (2011), relies on a multiresolution approach based on the elliptical polarization of Rayleigh waves, using three-component records to determine the instantaneous degree of elliptical polarization. It employs a variation of the degree of polarization (DOP) approach (Schimmel & Gallart, 2004) to extract elliptically polarized signals in a vertical plane. The DOP is calculated from the instantaneous ground motion ellipse and its temporal variations. Finally, it resolves the 180° ambiguity in the back azimuth (BAZ) assuming the retrograde motion of Rayleigh waves.



19448007, 2026, 12, Downloaded from https://agupubs.onlinelibrary.wiley.com/doi/10.1029/2025GL120829 by Portail BibCNRS INSU, Wiley Online Library on [03/11/2026]. See the Terms and Conditions (https://onlinelibrary.wiley.com/terms-and-conditions) on Wiley Online Library for rules of use; OA articles are governed by the applicable Creative Commons License

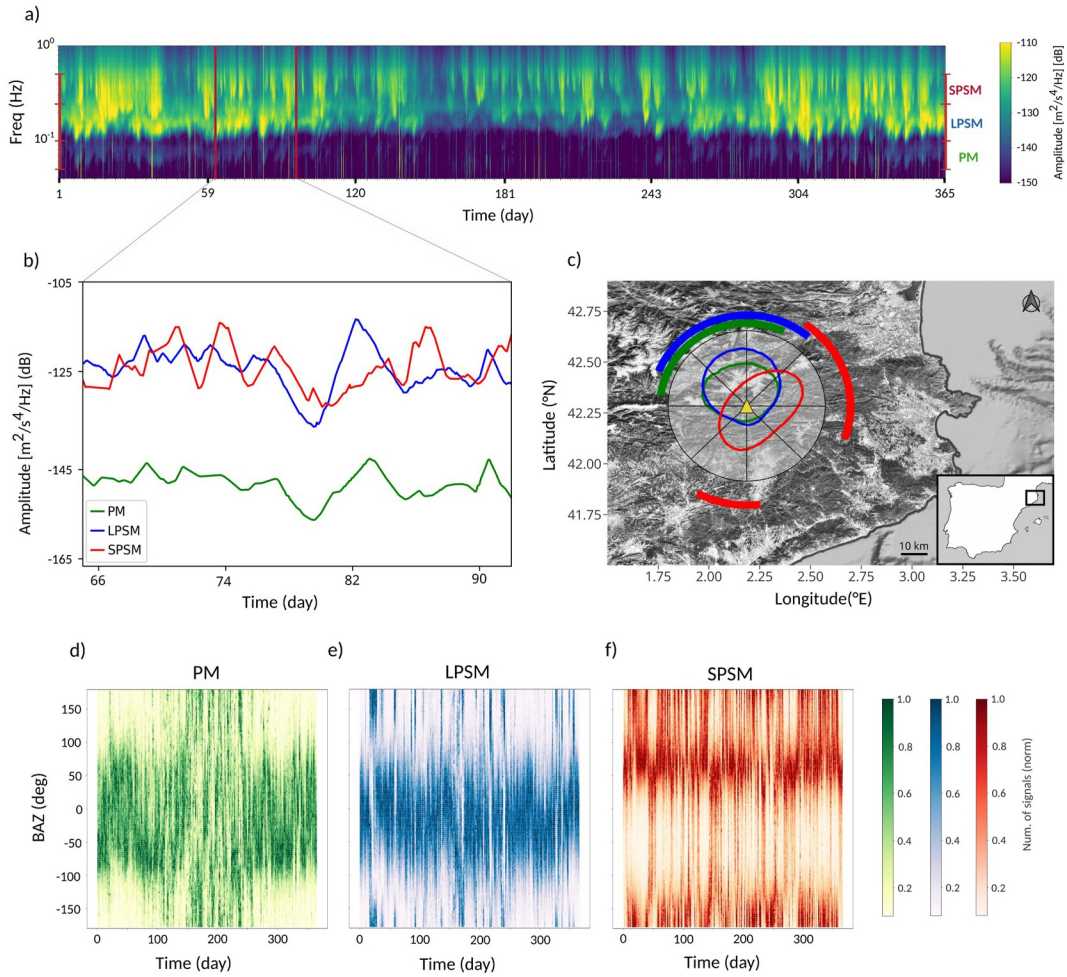



**Figure 1.** (a) 2023 CBRU spectrogram from 0.04 to 1 Hz marked with the different frequency ranges used in this study: PM from 0.05 to 0.1 Hz, long-period secondary microseism (LPSM) from 0.1 to 0.25 Hz and short-period secondary microseism (SPSM) from 0.25 to 0.5 Hz. (b) Mean energy values within this frequency ranges for 1 month (March 2023) (c) BAZs obtained for each one of the microseisms. The bars outside represent the directions from which the majority of Rayleigh waves arrive, based on the upper 30% of the detected signals. (d,e,f) The number of elliptically polarized signals obtained for PM (green), LPSM (blue) and SPSM (red) throughout 2023, as a function of time with a daily temporal resolution and BAZ with a 3° resolution. The signal counts are normalized with respect to the daily maximum.

### 2.3. Modeling the Energy Contribution of Source Regions to SM

As polarization results reveal distinct source regions for each microseismic peak, the energy contribution of each region to SM can be independently investigated through numerical simulations, providing cross-validation between distinct and independent methodologies. For this purpose, the Weakly Laterally Heterogeneous Media (WLHM) modeling approach (Xu et al., 2025) is employed to simulate the SM Power Spectral Density (PSD). This method improves the classic Laterally Homogeneous modeling (LH-SM) (Ardhuin et al., 2011, 2013; Gimbert & Tsai, 2015; Stutzmann et al., 2012) by incorporating WLHM Green's functions that account for ocean, sediment, and crustal layers at both the source and receiver, rather than assuming a laterally homogeneous two-layer model. This allows more accurate representation of Rayleigh-wave excitation at the source and amplitude amplification at the receiver due to sediment effects, reducing the risk of under- or overestimating ocean-wave energy. Further details of the modeling are provided in Text S1 in Supporting Information S1 and in Xu et al. (2025).

Although the maximum frequency analyzed in this study is 0.5 Hz, the modeling is limited to 0.33 Hz because Rayleigh waves can behave as Scholte waves above 0.3 Hz (Scholte, 1958). This limitation does not affect our



19448007, 2026, 12, Downloaded from https://agupubs.onlinelibrary.wiley.com/doi/10.1029/2025GL120829 by Portail BibCNRS INSU, Wiley Online Library on [03/11/2026]. See the Terms and Conditions (https://onlinelibrary.wiley.com/terms-and-conditions) on Wiley Online Library for rules of use; OA articles are governed by the applicable Creative Commons License

19448007, 2026, 12, Downloaded from https://agupubs.onlinelibrary.wiley.com/doi/10.1029/2025GL120829 by Portail BibCNRS INSU, Wiley Online Library on [03/11/2026]. See the Terms and Conditions (https://onlinelibrary.wiley.com/terms-and-conditions) on Wiley Online Library for rules of use; OA articles are governed by the applicable Creative Commons License

objectives, as this range captures all relevant observations. First, we run a model that includes all SM sources in the 0.1–0.33 Hz band to determine $Q$ (the Rayleigh-wave average quality factor) and $R^2$ (the average ocean wave reflection coefficient at shorelines), achieving good agreement with both our study and other Mediterranean stations. Using these parameters, we then rerun the modeling under two additional scenarios: one considering only the energy contribution of the Mediterranean Sea and another considering all SM sources except the Mediterranean Sea. Both cases highlight the importance of the Mediterranean Sea in SPSM generation.

For the source maps, we use the SM pressure source PSDs derived from WAVEWATCH III where the parameter is referred as "p2l" following Ardhuin et al. (2011). We then integrate over the time period we are interested in and over the SPSM frequency band (0.25–0.5 Hz). Finally, we compare these results with those including the bathymetry-dependent SM excitation coefficients for Rayleigh waves (Ardhuin et al., 2011; Gualtieri et al., 2013; Stutzmann et al., 2012), proposed by Longuet-Higgins (1950), to study the influence of bathymetry in the SPSM source generation and spatial distribution. Further details provided in Text S1 in Supporting Information S1.

### 2.4. SPSM Amplitude Attenuation

To better constrain the location of the SPSM sources within the Mediterranean Sea, we analyze its energy attenuation inland using the profiles described in Section 2.1. This provides a valuable opportunity, as both profiles consist of closely spaced stations located near the shoreline, allowing a detailed analysis of SPSM attenuation in different directions and over several tens of kilometers inland.

For this analysis, we use the vertical components of the seismometers, where Rayleigh waves are expected to be most clearly recorded. Rayleigh wave amplitude attenuates with distance due to both absorption and geometric spreading. Here absorption is not explicitly considered as the short inter-station distances result in minimal amplitude reduction; for example, using the Q value of 130 from our modeling, attenuation at 0.3 Hz with a phase velocity of 2 km/s is less than 15% along our 52 km profile, indicating that this effect is negligible along the profiles. Thus, we use geometric attenuation, which causes the amplitude to decrease roughly as $r^{-1/2}$, where $r$ is the distance from the source. Using the geometric attenuation for Rayleigh waves (Figure and text S2 in Supporting Information S1), along with the BAZs derived from the Rayleigh-wave polarization, we estimate a proxy for the offshore distance to the source.

## 3. Results and Interpretation

### 3.1. Disentangling Microseismic Source Regions

In the Mediterranean Sea the microseismic noise is characterized by a splitting of the SM into LPSM and SPSM (Figure 1a) visible in spectrograms all around the region. Unlike the LPSM, which is consistently present, the SPSM is intermittent. Seasonal variations between winter and summer can also be observed in the power spectra. This split is present across multiple years in this region (Figure S3 in Supporting Information S1). By representing the amplitude as the average energy level within each frequency band corresponding to the three microseismic peaks (Figure 1b), it is observed that PM and LPSM share a similar energy pattern as a function of time, whereas SPSM displays a distinctly different one. This suggests the presence of distinct source locations: a common source region for PM and LPSM and a separate one for SPSM.

We then perform the Rayleigh-wave polarization analysis for each of the three frequency bands (Figures 1d–1f) to study in detail the source regions of each microseismic peak. The results show that PM and LPSM exhibit nearly identical BAZs throughout the year, pointing toward the North Atlantic Ocean, while SPSM displays a distinct BAZ, oriented to the Mediterranean Sea (Figure 1c). This pattern is consistently observed across multiple years (Figure S3 in Supporting Information S1) and it is in good agreement with the previously observed energy distribution, also revealing two distinct source locations.

From this section we extract two key observations: (a) SM is consistently split into LPSM and SPSM in this region, and (b) we identify two distinct source locations: one in the North Atlantic Ocean for PM and LPSM, and another in the Mediterranean Sea for SPSM. This represents a great opportunity to study SPSM sources, as their energy is confined within the Mediterranean Sea without interference from sources in other regions.

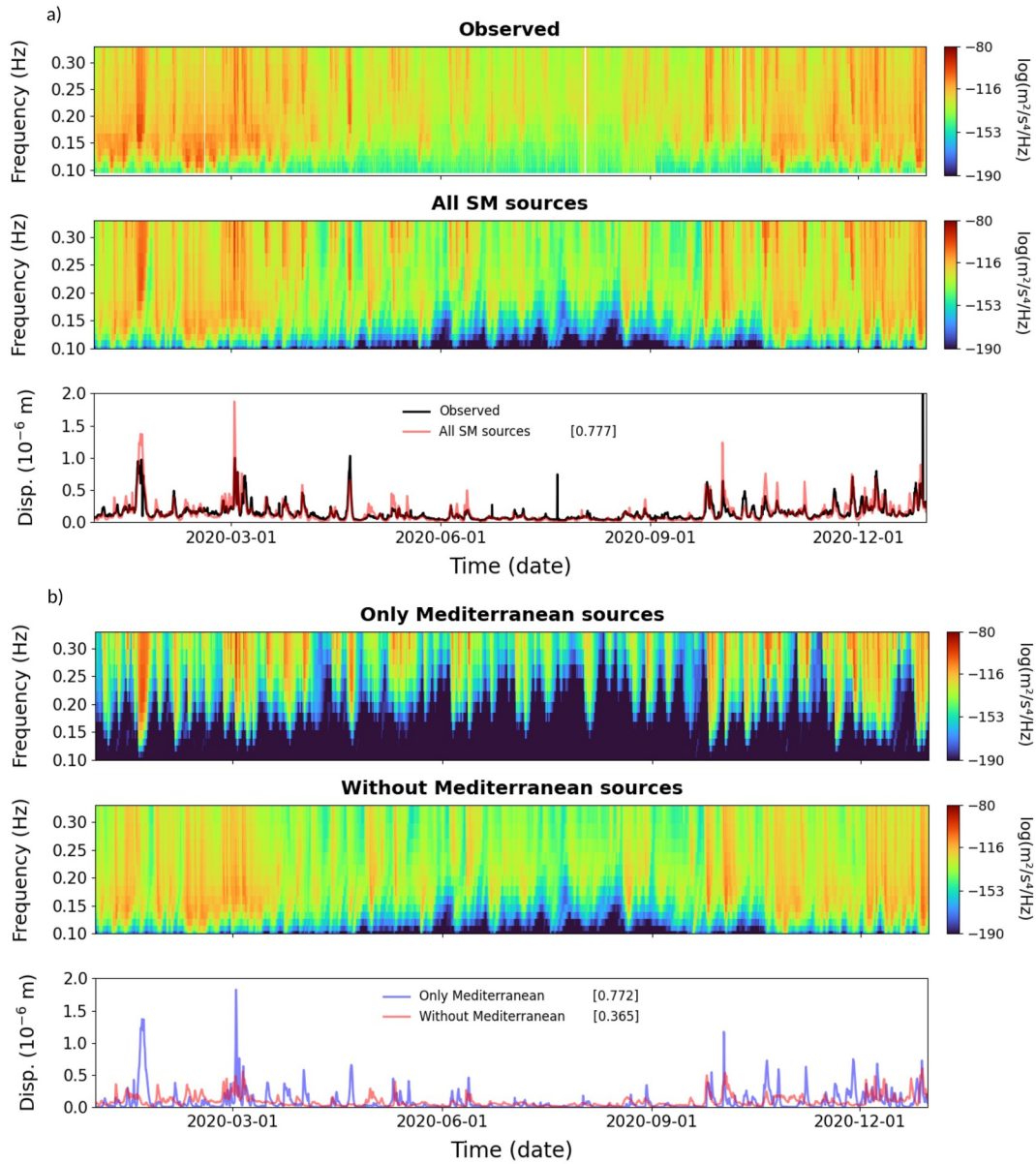



**Figure 2.** Observed and synthetic spectrograms from the weakly laterally heterogeneous media modeling approach for the CBRU permanent station during 2020, shown with mean displacement amplitude curves in the 0.2–0.33 Hz short-period secondary microseism band. Numbers in brackets represent the Pearson correlation coefficient relative to the observed curve. (a) Upper panels: observed and synthetic spectrogram including all SM sources; lower panel: displacement curves for the observed (black) and synthetic (red). (b) Upper panels: synthetic spectrograms including only the Mediterranean contribution or excluding it; lower panel: displacement curves for synthetics including (blue) or excluding (red) the Mediterranean.

### 3.2. Spatio-Temporal Modeling of SM Sources

The modeling results show that including all SM sources (Figure 2a) clearly captures LPSM energy in the 0.1–0.2 Hz range and SPSM energy above 0.2 Hz. Considering only the Mediterranean Sea (Figure 2b) causes the LPSM energy to disappear while SPSM energy persists. Conversely, excluding the Mediterranean while including all other sources preserves LPSM energy intact but significantly smooths the SPSM band and eliminates high-amplitude features above 0.2 Hz. These findings support the idea that LPSM energy recorded at our stations primarily originates from the North Atlantic Ocean, while SPSM is generated within the Mediterranean, and further emphasize that both can be explained by the same wave–wave interaction mechanism responsible for SM.



19448007, 2026, 12, Downloaded from https://agupubs.onlinelibrary.wiley.com/doi/10.1029/2025GL120829 by Portail BibCNRS INSU, Wiley Online Library on [03/11/2026]. See the Terms and Conditions (https://onlinelibrary.wiley.com/terms-and-conditions) on Wiley Online Library for rules of use; OA articles are governed by the applicable Creative Commons License

19448007, 2026, 12, Downloaded from https://agupubs.onlinelibrary.wiley.com/doi/10.1029/2025GL120829 by Portail BibCNRS INSU, Wiley Online Library on [03/11/2026]. See the Terms and Conditions (https://onlinelibrary.wiley.com/terms-and-conditions) on Wiley Online Library for rules of use; OA articles are governed by the applicable Creative Commons License

Analyzing the displacement amplitude curves in the 0.2–0.33 Hz band reveals good agreement between observed and synthetic data including all SM sources (Figure 2a), with a strong Pearson correlation coefficient. Some over- or underestimation at peaks is expected, as a single set of spatially averaged $Q$ and $R^2$ parameters is used for the entire year, which may not capture individual storms or specific time windows; however, this does not affect our conclusions. Using only the Mediterranean contribution yields nearly identical amplitude levels and correlation coefficient, whereas excluding it while including all other sources results in a significant energy loss in this band (Figure 2b). These results confirm that the Mediterranean Sea is the dominant SPSM source, with the North Atlantic and other secondary sources contributing only at background levels. The modeling results reach to the same interpretation as the polarization, identifying different microseismic source regions through distinct and independent methodologies.

### 3.3. Locating SPSM Sources

Having established that the SPSM energy originates within the Mediterranean Sea, we aim to better locate its sources using the two orthogonal profiles deployed in NE Iberia (Figure 3). The amplitude evolution shows that attenuation is more pronounced along the profile parallel to the coastline than along the orthogonal profile in the SPSM frequency band (Figure S4 in Supporting Information S1). This suggests that SPSM energy is not solely related to coastal proximity, and that distinct source regions may exist within the Mediterranean Sea.

Furthermore, along the parallel profile (Figure 3a), we identify a predominant attenuation in the NE–SW direction that is present most of the time. However, during certain time periods, this predominant attenuation direction reverses to the SW–NE direction (Figure 3a). This indicates that the location of the SPSM sources may also vary over time. To test this hypothesis, we apply the same Rayleigh-wave polarization as in Section 3.1, but this time focusing on short temporal windows corresponding to each one of the observed attenuation patterns (Figure 3a). This analysis reveals that, during the typical attenuation in the NE–SW direction, the SPSM BAZ lies between 90° and 110°, whereas during the reversed SW–NE direction, it shifts to between 135° and 220°, clearly pointing to the south. The lower attenuation and the same pattern can be seen in the orthogonal profile for this time period (Figure S5 in Supporting Information S1). These results demonstrate the presence of two distinct SPSM sources in this region: the main one to the east of the profiles and another to the south. Furthermore, these sources display strong and rapid temporal variability.

Using the source located toward the east of the profiles as a reference, we perform two additional analyses on 3 August 2024, where a clear maximum is observed: (a) we select two broad band stations located 45 km apart and apply the Rayleigh-wave polarization (Figure 3b). Both stations indicate convergence toward a common region located several kilometers offshore. (b) Using the principle of Rayleigh-wave geometric attenuation (Figure and Text S2 in Supporting Information S1) and the BAZs derived from the polarization approach, we estimate that this source is located roughly 30–40 km offshore, in the Gulf of Lion.

Now that we have identified a SPSM source in the Gulf of Lion, constrained by the BAZ and distance estimation, we aim to assess whether the wave model accurately captures the source location during this time period, comparing it also with the mean significant wave height (Figure 3c). First, we integrate the SM pressure source PSDs (Figure 3d) over time (for this day) and over the SPSM frequency band (0.25–0.5 Hz). Then, the bathymetry-dependent SM excitation coefficients for Rayleigh waves have been included. The results (Figure 3e) indicate that, when bathymetry is taken into account, an isolated and well-defined SPSM source arises in the Gulf of Lion, consistent with the distances and BAZs obtained using both the polarization and amplitude attenuation approaches. Comparing this source location with the mean significant wave height during this time period, it is observed that the source does not correspond to the highest wave heights, but rather to a more localized area where the bathymetry is favorable for SPSM generation. The same approach is applied to the previous source activations in Figure 3a, associated with different storms (Figures S6 and S7 in Supporting Information S1).

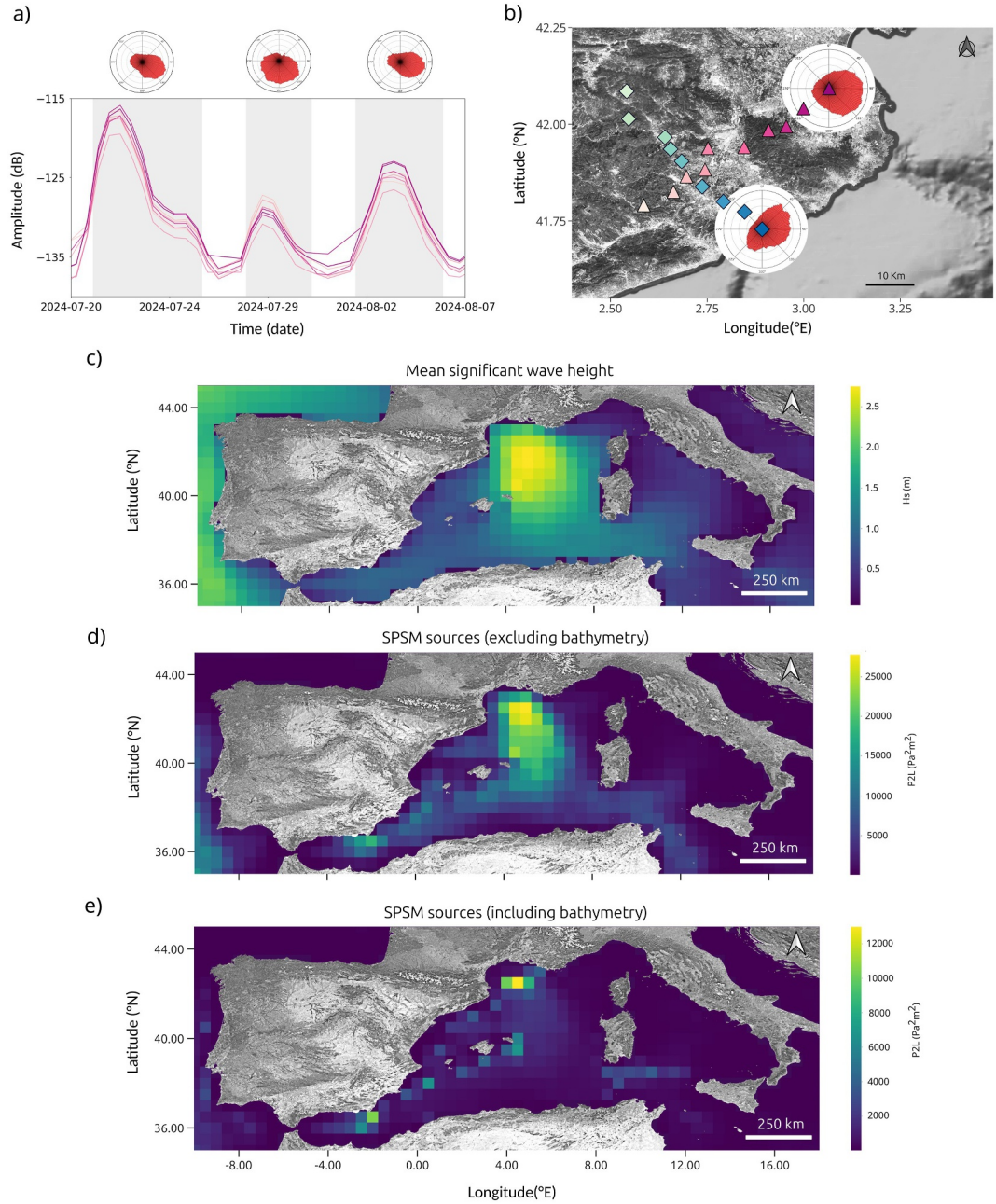



**Figure 3.** (a) 18 days from the parallel profile, highlighting the two typical attenuation patterns and the corresponding BAZs derived from Rayleigh-wave polarization for the nearest station to the shoreline within the shaded areas. During the maximum on 3 August: (b) map with the two station profiles and the BAZs estimated from the nearest coastal stations, (c) mean significant wave height during this day, (d) SM pressure source power spectral density map integrated over time (for the day) and frequency (0.25–0.5 Hz); and (e) the same as (d) but including the bathymetry-dependent SM excitation coefficients.

## 4. Discussion and Conclusions

In this study, we observe a splitting of the SM signal recorded at stations in the Mediterranean region into LPSM and SPSM, consistent over different years (Figure S3 in Supporting Information S1) and regions (Figure 4). Additionally, we demonstrate through a Rayleigh-wave polarization the presence of two distinct source locations: one in the North Atlantic Ocean, responsible for PM and LPSM, and another within the Mediterranean Sea, responsible for SPSM. This microseismic source distribution can be homogeneously identified across multiple



19448007, 2026, 12, Downloaded from https://agupubs.onlinelibrary.wiley.com/doi/10.1029/2025GL120829 by Portail BibCNRS INSU, Wiley Online Library on [03/11/2026]. See the Terms and Conditions (https://onlinelibrary.wiley.com/terms-and-conditions) on Wiley Online Library for rules of use; OA articles are governed by the applicable Creative Commons License

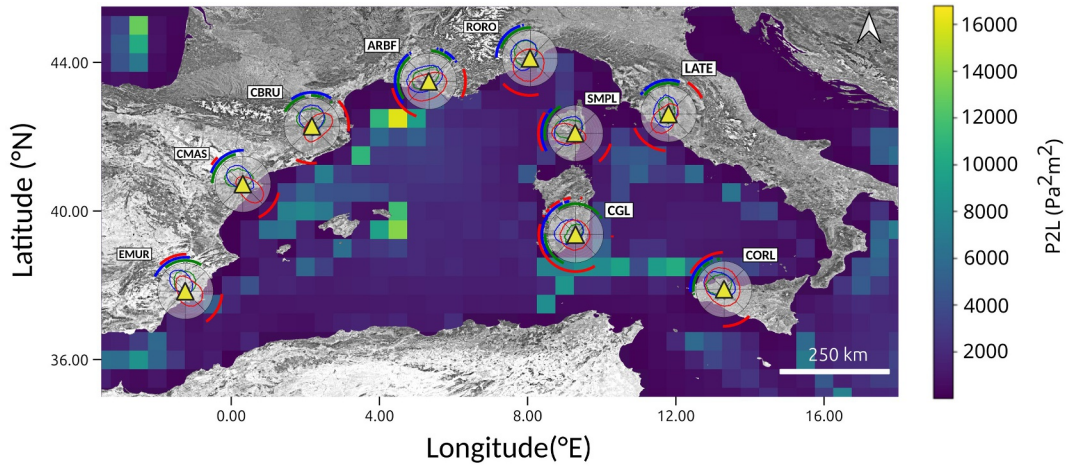



**Figure 4.** BAZs for different stations across Europe showing the PM (green), long-period secondary microseism (blue) and short-period secondary microseism (SPSM) (red) during the first 60 days of 2023. The bars outside the polar graphs represent the 20% of BAZs with most signals recorded for each kind of microseism. In the SPSM case, we also consider the secondary maxima to capture additional features from other secondary sources. In the CGL station, due to the highly isotropic SPSM polarization, the upper 20% of the normalized range was used as a threshold to avoid spurious directional clustering. The SM pressure source power spectral density (PSD) map including the bathymetry-dependent excitation coefficients, is also shown. The PSD map is integrated over the 60-day period represented by the BAZs and over the 0.25–0.5 Hz frequency band.

stations throughout the Mediterranean (Figure 4). The SM source modeling carried out in this study allows us to independently study the energy contribution of each microseismic region, obtaining consistent results through different and independent methodologies. The local differences in the PM and LPSM BAZs observed at stations located relatively close to each other, such as CBRU and CMAS, may be influenced by local or regional structure which may cause directional attenuation or multipathing, for instance, by the Pyrenees in analogy to previous observations seen for the Alps (Campillo et al., 1993). A similar pattern is noted in the SPSM signal, where a maximum pointing toward the Atlantic Ocean is observed at the EMUR station, while it is not apparent at the CBRU station, despite the former being located more than 300 km further inland.

This split in the microseismic source distribution allows us to explain why Borzì et al. (2025) report low Spearman correlation coefficients between PM and LPSM amplitudes with wave heights when focusing on the Mediterranean region. It is also in good agreement with previous works, such as Stehly et al. (2024), which identify energy arriving from different regions of the Atlantic Ocean and the Mediterranean. In this study, however, we provide a more detailed characterization of the frequency bands and azimuths of the energy associated with each source region. Notably, PM is consistently recorded from the North Atlantic Ocean across the entire western Mediterranean (Figure 4). This is expected, even though the Mediterranean Sea can generate waves with periods longer than 10 s, the dominant wave periods are generally lower, around 4 s (Coppini et al., 2023). Thus, the energy within the selected frequency range for PM is dominated by signals originating from the North Atlantic Ocean. The local PM energy generated in the Mediterranean Sea is likely masked by the LPSM, as observed in other marginal seas such as the North Sea (Becker et al., 2020). This represents wave periods between 4 and 8 s as those expected for the local PM in the Mediterranean. However, in this study we focus on analyzing the dominant signals that can be identified in the spectra recorded at stations across the region (Figure S1 in Supporting Information S1).

To our knowledge, it is the first time that Rayleigh-wave polarization analysis is applied in the Mediterranean Sea in combination with SM source modeling to characterize microseismic noise. This approach allows us not only to discriminate between the two microseismic source regions, but also to reveal that the SPSM sources are well constrained and spatially localized with preferred incoming directions unrelated to the nearest coastal segments. These findings highlight the importance of polarization analysis for locating noise sources, particularly in contexts where other methodologies, such as DAS, cannot apply it, leading to misinterpretations.

We identify two distinct attenuation patterns in the profiles located in NE Iberia, where the BAZs suggest two different SPSM sources in this region: the main one in the Gulf of Lion and a second one located in the south.



19448007, 2026, 12, Downloaded from https://agupubs.onlinelibrary.wiley.com/doi/10.1029/2025GL120829 by Portail BibCNRS INSU, Wiley Online Library on [03/11/2026]. See the Terms and Conditions (https://onlinelibrary.wiley.com/terms-and-conditions) on Wiley Online Library for rules of use; OA articles are governed by the applicable Creative Commons License

19448007, 2026, 12, Downloaded from https://agupubs.onlinelibrary.wiley.com/doi/10.1029/2025GL120829 by Portail BibCNRS INSU, Wiley Online Library on [03/11/2026]. See the Terms and Conditions (https://onlinelibrary.wiley.com/terms-and-conditions) on Wiley Online Library for rules of use; OA articles are governed by the applicable Creative Commons License

Focusing on the Gulf of Lion source on 3 August 2024, where a clear maximum is observed, we use the BAZ obtained together with Rayleigh wave geometric attenuation to estimate a proxy for the source distance of 30–40 km offshore (Figure and text S2 in Supporting Information S1). Based on previous studies in the Mediterranean Sea that analyze the frequency content of SPSM sources under both normal and extreme events, the storms examined here might be classified as normal storms, with SPSM frequencies around 0.3–0.35 Hz (Borzì et al., 2024).

Beyond their frequency content, SPSM amplitudes are also linked to storm intensity (Cutroneo et al., 2021; Ferretti et al., 2013). Although it is well known that higher wave heights cannot be directly correlated with stronger SM sources (Obrebski et al., 2012), the SM pressure source PSD map obtained for this time period (Figure 3d) shows a good correlation with the mean significant wave height (Figure 3c). This is expected, as marginal seas such as the Mediterranean, characterized by relatively short distances, may not exhibit a clear distinction between regions of higher wave heights and the location of stronger SM sources.

In contrast, when the bathymetry-dependent SM excitation coefficients for Rayleigh waves, proposed by Longuet-Higgins (1950), are integrated into the model (Figure 3e), a much more localized source arises, consistent with the measured BAZs and the inferred distances. These results demonstrate the importance of bathymetry in the generation and spatial distribution of SPSM sources. This approach is also applied to different storm events during the source activation periods identified in Figure 3a (Figures S6 and S7 in Supporting Information S1). The existence of a recurrent source in the Gulf of Lion would explain the consistently similar BAZs observed throughout the year (Figure 1f) and across different years (Figure S3 in Supporting Information S1) in NE Iberia.

Furthermore, earlier works, such as Gal et al. (2017), have suggested that convex shoreline geometries can promote the occurrence of SM mechanisms. To explore this, we ran preliminary models (not shown here) to assess whether the Gulf of Lion's convex shape influences the SM generation. Our results indicate that, based on energy reflections alone, the Gulf of Lion may generate one of the strongest SM sources in the Mediterranean Sea. Thus, this SPSM source likely results from a combination of two factors: (a) reflections along the convex shoreline promoting a SM mechanism, and (b) spatial distribution controlled by bathymetry.

Extending our analysis to the western Mediterranean and incorporating the depth-dependent excitation coefficients (Figure 4), we identify a correlation between SPSM BAZs across multiple stations and distinct SPSM source regions. The RORO station may present slight misorientation of its horizontal components and/or a limited number of elliptically polarized signals, which could affect the robustness of the observations. Furthermore, the identified sources do not exhibit any clear correlation with the mean significant wave height over the same period (Figure S8 in Supporting Information S1). As the time interval considered becomes longer, the distinction between maximum wave heights and the location of the sources becomes more evident, which also reveals an association of these sources with shallow bathymetries. These results further support both the importance of polarization for locating SPSM sources and the role of bathymetry in controlling their spatial distribution.

## Conflict of Interest

The authors declare no conflicts of interest relevant to this study.

## Availability Statement

The seismic data set used in this study, from stations in Spain, France and Italy, is publicly available through the Orfeus EIDA web services (https://www.orfeus-eu.org/data/eida) under the network codes CA (Institut Cartogràfic i Geològic de Catalunya, 1984), ES (Instituto Geografico Nacional, Spain, 1999), FR (Epos-France, 1962), IV (Istituto Nazionale di Geofisica e Vulcanologia (INGV), 2005) and GU (University of Genoa, 1967). The complete seismic data set acquired by the temporary YH network (Diaz & Schimmel, 2024) will be publicly distributed through the Institute Cartogràfic I Geològic de Catalunya (ICGC) EIDA Data Center (http://ws.icgc.cat/fdsnws) after the embargo period, but the data used in this study are already available at Díaz et al. (2026). The polarization software is available at Schimmel and Stutzmann (2019) and the SM modeling code at Xu (2025).

**Acknowledgments**
We acknowledge the GEO3BCN-CSIC LabSis Laboratory (http://labsis.geo3bcn.csic.es) for providing their signal processing capacities. We also thank ORFEUS EIDA (http://www.orfeus-eu.org/data/eida) for providing easy access to seismic data, the editor Germán Prieto for handling the manuscript, and the reviewers, Sebastiano D'Amico and an anonymous reviewer, for their constructive comments, which helped improve the manuscript. This is a contribution of the EPYSIM Project, funded by the Spanish Ministry of Science and Innovation (Ref.: PID2022-136981NB-100). Samuel Jorde benefits from a pre-doctoral Grant from the Spanish Ministry of Science and Innovation (Ref.: PREP2022-000593).

## References

Ardhuin, F., Gualtieri, L., & Stutzmann, E. (2015). How ocean waves rock the Earth: Two mechanisms explain microseisms with periods 3 to 300 s. *Geophysical Research Letters*, *42*(3), 765–772. https://doi.org/10.1002/2014gl062782

Ardhuin, F., Lavanant, T., Obrebski, M., Marié, L., Royer, J.-Y., d'Eu, J.-F., et al. (2013). A numerical model for ocean ultra-low frequency noise: Wave-generated acoustic-gravity and rayleigh modes. *Journal of the Acoustical Society of America*, *134*(4), 3242–3259. https://doi.org/10.1121/1.4818840

Ardhuin, F., Stutzmann, E., Schimmel, M., & Mangeney, A. (2011). Ocean wave sources of seismic noise. *Journal of Geophysical Research*, *116*(C9), C09004. https://doi.org/10.1029/2011jc006952

Becker, D., Cristiano, L., Peikert, J., Kruse, T., Dethof, F., Hadziioannou, C., & Meier, T. (2020). Temporal modulation of the local microseism in the north sea. *Journal of Geophysical Research: Solid Earth*, *125*(10), e2020JB019770. https://doi.org/10.1029/2020jb019770

Borzì, A. M., Cannata, A., Panzera, F., D'Amico, S., Lo Re, C., & Aster, R. C. (2025). Microseism amplitude and wave power in the Mediterranean Sea (1996–2023). *Journal of Geophysical Research: Solid Earth*, *130*(1), e2024JB030528. https://doi.org/10.1029/2024jb030528

Borzì, A. M., Minio, V., De Plaen, R., Lecocq, T., Cannavò, F., Ciraolo, G., et al. (2024). Long-term analysis of microseism during extreme weather events: Medicanes and common storms in the Mediterranean Sea. *Science of the Total Environment*, *915*, 169989. https://doi.org/10.1016/j.scitotenv.2024.169989

Bromirski, P. D., Duennebier, F. K., & Stephen, R. A. (2005). Mid-ocean microseisms. *Geochemistry, Geophysics, Geosystems*, *6*(4), Q04009. https://doi.org/10.1029/2004gc000768

Campillo, M., Feignier, B., Bouchon, M., & Béthoux, N. (1993). Attenuation of crustal waves across the alpine range. *Journal of Geophysical Research*, *98*(B2), 1987–1996. https://doi.org/10.1029/92jb02357

Coppini, G., Clementi, E., Cossarini, G., Salon, S., Korres, G., Ravdas, M., et al. (2023). The mediterranean forecasting system–part 1: Evolution and performance. *Ocean Science*, *19*(5), 1483–1516. https://doi.org/10.5194/os-19-1483-2023

Cutroneo, L., Ferretti, G., Barani, S., Scafidi, D., De Leo, F., Besio, G., & Capello, M. (2021). Near real-time monitoring of significant sea wave height through microseism recordings: Analysis of an exceptional sea storm event. *Journal of Marine Science and Engineering*, *9*(3), 319. https://doi.org/10.3390/jmse9030319

Davy, C., Stutzmann, E., Barruol, G., Fontaine, F. R., & Schimmel, M. (2015). Sources of secondary microseisms in the Indian Ocean. *Geophysical Journal International*, *202*(2), 1180–1189. https://doi.org/10.1093/gji/ggv221

Diaz, J., Jara, J.-A., Sánchez-Pastor, P., Frontera, T., Seivane, H., Jorde, S., & Lecocq, T. (2025). Monitoring time variations in seismic noise amplitude at permanent seismic networks. *Seismica*, *4*(1). https://doi.org/10.26443/seismica.v4i1.1408

Diaz, J., & Schimmel, M. (2024). Epysim [Dataset]. *International Federation of Digital Seismograph Networks*. https://doi.org/10.7914/NF26-A458

Díaz, J., Schimmel, M., Jorde, S., & Ruiz, M. (2026). Seismic profile data [Dataset]. *Zenodo*. https://doi.org/10.5281/zenodo.19698198

Epos-France. (1962). Epos-france broad-band network (RLBP) [Dataset]. *Epos-France Seismological Data Centre*. https://doi.org/10.15778/RESIF.FR

Ermert, L., Sager, K., Afanasiev, M., Boehm, C., & Fichtner, A. (2017). Ambient seismic source inversion in a heterogeneous Earth: Theory and application to the earth's hum. *Journal of Geophysical Research: Solid Earth*, *122*(11), 9184–9207. https://doi.org/10.1002/2017jb014738

Ermert, L., Villasenor, A., & Fichtner, A. (2016). Cross-correlation imaging of ambient noise sources. *Geophysical Journal International*, *204*(1), 347–364. https://doi.org/10.1093/gji/ggv460

Ferretti, G., Zunino, A., Scafidi, D., Barani, S., & Spallarossa, D. (2013). On microseisms recorded near the Ligurian Coast (Italy) and their relationship with sea wave height. *Geophysical Journal International*, *194*(1), 524–533. https://doi.org/10.1093/gji/ggt114

Gal, M., Reading, A., Ellingsen, S., Koper, K., & Burlacu, R. (2017). Full wavefield decomposition of high-frequency secondary microseisms reveals distinct arrival azimuths for rayleigh and love waves. *Journal of Geophysical Research: Solid Earth*, *122*(6), 4660–4675. https://doi.org/10.1002/2017jb014141

Gimbert, F., & Tsai, V. C. (2015). Predicting short-period, wind-wave-generated seismic noise in coastal regions. *Earth and Planetary Science Letters*, *426*, 280–292. https://doi.org/10.1016/j.epsl.2015.06.017

Gualtieri, L., Stutzmann, E., Capdeville, Y., Ardhuin, F., Schimmel, M., Mangeney, A., & Morelli, A. (2013). Modelling secondary microseismic noise by normal mode summation. *Geophysical Journal International*, *193*(3), 1732–1745. https://doi.org/10.1093/gji/ggt090

Gualtieri, L., Stutzmann, É., Farra, V., Capdeville, Y., Schimmel, M., Ardhuin, F., & Morelli, A. (2014). Modelling the ocean site effect on seismic noise body waves. *Geophysical Journal International*, *197*(2), 1096–1106. https://doi.org/10.1093/gji/ggu042

Hasselmann, K. (1963). A statistical analysis of the generation of microseisms. *Reviews of Geophysics*, *1*(2), 177–210. https://doi.org/10.1029/rg001i002p00177

Haubrich, R. A., & McCamy, K. (1969). Microseisms: Coastal and pelagic sources. *Reviews of Geophysics*, *7*(3), 539–571. https://doi.org/10.1029/rg007i003p00539

Institut Cartogràfic i Geològic de Catalunya. (1984). Catalan seismic network [Dataset]. *International Federation of Digital Seismograph Networks*. https://doi.org/10.7914/SN/CA

Instituto Geografico Nacional, Spain. (1999). Spanish digital seismic network [Dataset]. *International Federation of Digital Seismograph Networks*. https://doi.org/10.7914/SN/ES

Istituto Nazionale di Geofisica e Vulcanologia (INGV). (2005). Rete sismica nazionale (RSN) [Dataset]. *Istituto Nazionale di Geofisica e Vulcanologia (INGV)*. https://doi.org/10.13127/SD/X0FXNH7QFY

Kedar, S., Longuet-Higgins, M., Webb, F., Graham, N., Clayton, R., & Jones, C. (2008). The origin of deep ocean microseisms in the north Atlantic Ocean. *Proceedings of the Royal Society A: Mathematical, Physical and Engineering Sciences*, *464*(2091), 777–793. https://doi.org/10.1098/rspa.2007.0277

Koper, K. D., & Burlacu, R. (2015). The fine structure of double-frequency microseisms recorded by seismometers in North America. *Journal of Geophysical Research: Solid Earth*, *120*(3), 1677–1691. https://doi.org/10.1002/2014jb011820

Longuet-Higgins, M. S. (1950). A theory of the origin of microseisms. *Philosophical Transactions of the Royal Society of London. Series A, Mathematical and Physical Sciences*, *243*(857), 1–35. https://doi.org/10.1098/rsta.1950.0012

Meschede, M., Stutzmann, É., Farra, V., Schimmel, M., & Ardhuin, F. (2017). The effect of water column resonance on the spectra of secondary microseism p waves. *Journal of Geophysical Research: Solid Earth*, *122*(10), 8121–8142. https://doi.org/10.1002/2017jb014014

Möllhoff, M., & Bean, C. J. (2016). Seismic noise characterization in proximity to strong microseism sources in the northeast Atlantic. *Bulletin of the Seismological Society of America*, *106*(2), 464–477. https://doi.org/10.1785/0120150204

Obrebski, M., Ardhuin, F., Stutzmann, E., & Schimmel, M. (2012). How moderate sea states can generate loud seismic noise in the deep ocean. *Geophysical Research Letters*, *39*(11), L11601. https://doi.org/10.1029/2012gl051896



19448007, 2026, 12, Downloaded from https://agupubs.onlinelibrary.wiley.com/doi/10.1029/2025GL120829 by Portail BibCNRS INSU, Wiley Online Library on [03/11/2026]. See the Terms and Conditions (https://onlinelibrary.wiley.com/terms-and-conditions) on Wiley Online Library for rules of use; OA articles are governed by the applicable Creative Commons License

Schimmel, M., & Gallart, J. (2004). Degree of polarization filter for frequency-dependent signal enhancement through noise suppression. *Bulletin of the Seismological Society of America*, *94*(3), 1016–1035. https://doi.org/10.1785/0120030178

Schimmel, M., & Stutzmann, E. (2019). Polfre: A time-frequency dependent polarization tool [Software]. https://doi.org/10.20350/digitalCSIC/13840

Schimmel, M., Stutzmann, E., Ardhuin, F., & Gallart, J. (2011). Polarized earth's ambient microseismic noise. *Geochemistry, Geophysics, Geosystems*, *12*(7), Q07014. https://doi.org/10.1029/2011gc003661

Scholte, J. G. J. (1958). Rayleigh waves in isotropic and anistropic elastic media. *Meded. Verhand. KNMI*, *72*, 9–43.

Sergeant, A., Stutzmann, E., Maggi, A., Schimmel, M., Ardhuin, F., & Obrebski, M. (2013). Frequency-dependent noise sources in the north Atlantic ocean. *Geochemistry, Geophysics, Geosystems*, *14*(12), 5341–5353. https://doi.org/10.1002/2013gc004905

Stehly, L., Delouche, E., Tomasetto, L., & Ranjan, P. (2024). Dynamic of seismic noise sources in the Mediterranean Sea: Implication for monitoring using noise correlations. Comptes rendus. *Geoscience*, *356*(S4), 1–24.

Stutzmann, E., Ardhuin, F., Schimmel, M., Mangeney, A., & Patau, G. (2012). Modelling long-term seismic noise in various environments. *Geophysical Journal International*, *191*(2), 707–722. https://doi.org/10.1111/j.1365-246x.2012.05638.x

Stutzmann, E., Schimmel, M., Patau, G., & Maggi, A. (2009). Global climate imprint on seismic noise. *Geochemistry, Geophysics, Geosystems*, *10*(11), Q11004. https://doi.org/10.1029/2009gc002619

University of Genoa. (1967). Regional seismic network of north Western Italy [Dataset]. *International Federation of Digital Seismograph Networks*. https://doi.org/10.7914/SN/GU

Xiao, H., Tanimoto, T., Spica, Z. J., Gaite, B., Ruiz-Barajas, S., Pan, M., & Viens, L. (2022). Locating the precise sources of high-frequency microseisms using distributed acoustic sensing. *Geophysical Research Letters*, *49*(17), e2022GL099292. https://doi.org/10.1029/2022gl099292

Xiao, H., Tanimoto, T., Spica, Z. J., & Tilmann, F. (2025). Frequency dependent microseisms sources: A case study in Oregon. *Geophysical Research Letters*, *52*(19), e2025GL118297. https://doi.org/10.1029/2025gl118297

Xu, Z. (2025). Matlab codes for 'theoretical modelling of secondary microseisms considering source and receiver site structures, with a focus on ocean-bottom sediment effects [Software]. *Zenodo*. https://doi.org/10.5281/zenodo.14832782

Xu, Z., Stutzmann, É., Farra, V., & Crawford, W. C. (2025). Theoretical modeling of secondary microseisms considering source and receiver site structures, with a focus on ocean-bottom sediment effects. *Journal of Geophysical Research: Solid Earth*, *130*(5), e2024JB030767. https://doi.org/10.1029/2024jb030767



19448007, 2026, 12, Downloaded from https://agupubs.onlinelibrary.wiley.com/doi/10.1029/2025GL120829 by Portail BibCNRS INSU, Wiley Online Library on [03/11/2026]. See the Terms and Conditions (https://onlinelibrary.wiley.com/terms-and-conditions) on Wiley Online Library for rules of use; OA articles are governed by the applicable Creative Commons License